Modeling the non-trivial behavior of anisotropic beams: a simple Timoshenko beam with enhanced stress recovery and constitutive relations

Giuseppe Balduzzi[a,*], Simone Morganti[b], Josef Füssl[a], Mehdi Aminbaghai[a], Alessandro Reali[c], Ferdinando Auricchio[c]

[a] *Institute for Mechanics of Materials and Structures (IMWS), Vienna University of Technology, Vienna, Austria*
[b] *Department of Electrical, Computer, and Biomedical Engineering, University of Pavia, Pavia, Italy*
[c] *Department of Civil Engineering and Architecture (DICAr), University of Pavia, Pavia, Italy*

Abstract

In this work we analyze the non-trivial influence of material anisotropy on the structural behavior of a multi-layer planar beam. Indeed, analytical results available in literature are limited to homogeneous beams and several aspects have not been addressed yet, preventing a deep understanding of the mechanical response of anisotropic structural elements. This paper proposes an effective recovery of stress distributions and an energetically consistent evaluation of constitutive relations to be used within a planar Timoshenko beam model. The resulting structural analysis tool highlights the following peculiarities of anisotropic beams: (i) the transversal internal force affects the maximum axial stress up to 30 %, and (ii) the anisotropy influences the beam displacements more than the standard shear deformation, even for extremely slender beams. A rigorous comparison with analytical and accurate 2D Finite Element solutions confirms the accuracy of the proposed approach, which leads to errors usually below 2 %.

Keywords: Anisotropic multi-layer beam, First Order Shear Deformation Theory, Analytical solution, Stress recovery, Beam constitutive relation

1. Introduction

Effective analysis and design of timber and composite structures unavoidably require beam and plate models capable to handle the material anisotropy. Nowadays, the need of accurate analysis tools is even more urgent due to the fast development of novel technologies. As an example, additive manufacturing allows the production of structural elements with variable orientation of fibers [20, 38]. Likewise, grain orientation distribution on the surfaces of timber boards can be derived from laser scanning data, allowing, for example, an accurate analysis [27, 33] and advanced optimization [40] of glued laminated timber beams.

*Corresponding author. *Address*: Institute for Mechanics of Materials and Structures (IMWS), Vienna University of Technology, Karlsplatz 13/202 A-1040 Vienna, Austria *Email address*: Giuseppe.Balduzzi@tuwien.ac.at *Phone*: 0043 (1) 58 80 12 02 28

Email addresses: Giuseppe.Balduzzi@tuwien.ac.at (Giuseppe Balduzzi), simone.morganti@unipv.it (Simone Morganti), Josef.Fuessl@tuwien.ac.at (Josef Füssl), Mehdi.Aminbaghai@tuwien.ac.at (Mehdi Aminbaghai), alessandro.reali@unipv.it (Alessandro Reali), ferdinando.auricchio@unipv.it (Ferdinando Auricchio)

Engineering research has spent great effort in beam and plate modeling within the last decades. Nevertheless, most models were derived under the hypothesis of isotropic or, at most, orthotropic material behavior [46, 11]. As a consequence, several features of anisotropic structural elements are not yet well addressed, in particular when principal directions of the material are not aligned with the beam axis or the plate reference surface.

Limiting the discussion to planar problems, the generalized 2D Hooke's law for isotropic material is represented by a block diagonal matrix. Consistently, beam constitutive relations are represented by a diagonal matrix i.e., axial strain, curvature, and shear strain uniquely depend on axial internal force, bending moment, and transversal internal force, respectively. Conversely, anisotropy leads the generalized 2D Hooke's law to be represented by a full matrix [31]. As a consequence, also constitutive relations for anisotropic structural elements may be represented by a full matrix, i.e., all generalized strains may depend on all internal forces.

Despite its importance, the above-mentioned issue was only partially addressed in literature. Murakami et al. [36] proposed a First-order Shear Deformation Theory (FSDT) for a planar homogeneous anisotropic beam, where a coupling term (mentioned also as coefficient of mutual influence [35, 34]) relates axial strain with shear force (and vice-versa). In the following years, several researchers [37, 26, 41, 45, 35] used different approaches for the estimation of the coupling term, reaching slightly different solutions. As will be discussed in the following, the introduction of a single coupling term allows models to be defined only for an extremely limited set of cross-section geometries, while simple and effective models capable of handling more general cases have not been proposed yet.

More recently, Karttunen and Von Hertzen [28] have proposed an accurate analysis of the structural behavior of an homogeneous anisotropic planar beam. The analytical expression for the stress distribution is calculated using the Airy's stress function, the analytical expression for strains is computed using 2D constitutive relations, and the 2D displacement field is recovered using the compatibility Partial Differential Equations (PDEs). Simple calculations allow the obtained analytical expression for 2D displacements and stresses to be reformulated in terms of 1D functions coinciding with internal forces and FSDT kinematic parameters. Taking advantage of this simplification, the authors provide the analytical expression of the Finite Element (FE) stiffness matrix of the beam. Analogously, stress distributions were obtained also by Hashin [23]. Nevertheless, the simplification proposed by Karttunen and Von Hertzen [28] highlights that the axial stress explicitly depends on the transversal internal force due to the non-trivial constitutive relations of the material. The above discussed analytical results represent a milestone for the development of effective anisotropic beams. However, the derivation procedure can not be easily generalized to multi-layer structures, significantly reducing the practical applicability.

Another important aspect that has to be handled carefully is the length of zones where boundary effects vanish according to the Saint-Venant principle [30, 3]. While for isotropic beams boundary effects are negligible at a distance greater than the maximum size of the cross-section, for anisotropic beams this distance depends on the ratio between axial and shear modulus and may be greater than six or seven times the maximum cross-section dimension [12, 9, 24]. Such a situation may strongly influence the buckling resistance of anisotropic structural elements [17] that can be effectively handled by means of suitable analysis techniques, like generalized eigenvectors method [19] or the generalized beam model [18]. Both the anisotropy and the boundary layer dimension have also an important effect approaching micro- and nano-scales, for which enhanced techniques, like the gradient elasticity theory, are needed [1, 2]. Limiting the discussion to FSDT, boundary effects reduce the effectiveness of beam models and introduce further phenomena that need to be considered in the analysis of structural elements, preventing a straightforward interpretation of both numerical and experimental results.

Nowadays, effective and accurate cross-section analysis tools (e.g., Variational Asymptotic Beam Sectional Analysis [47, 48, 42, 22], Semi-Analytical Finite Element [15, 29, 32, 14], Generalized Beam Theory [43], as well as plate models [21]) able to accurately handle the so far introduced problems are available. Nevertheless, all the cross-section analysis tools are based on auxiliary PDEs and functionals, which do not allow a direct physical interpretation of the analysis results. As a consequence, engineers usually use the above-mentioned analysis tools as black-boxes. Furthermore, the poor awareness of anisotropy effects on the structural behavior makes engineers erroneously believe that coarse adaptations of isotropic beam models

are effective [7].

The present paper proposes a simple planar beam model that effectively describes the linear elastic behavior of anisotropic multi-layer structural elements, accounting for the previously introduced issues. Specifically, the beam model will assume that the beam cross-section behaves rigidly, in analogy to the Timoshenko beam. If, on the one hand, this choice limits the accuracy and the applicability of the proposed beam model, on the other hand, it leads to Ordinary Differential Equations (ODEs) for which an analytical solution can be computed and easily interpreted by simple physical considerations, allowing a deep understanding of the structural behavior of anisotropic beams.

The main novelty of the developed model is an enhanced and effective stress recovery based on a two-stage iteration process. The first stage consists in exploiting the 2D constitutive relation for the recovery of axial stresses to take into account the effects of anisotropy on stress distribution. The second stage is based the horizontal equilibrium PDE for the recovery of shear stress, in analogy with the standard Jourawski approach [25, 10]. The proposed procedure can be extended to multi-layered anisotropic beams, allowing the evaluation of the non-trivial and explicit dependence of axial stresses on transversal internal force as well as on the applied external load. Beam constitutive relations are derived from the stress potential taking into account the stresses obtained from the introduced stress recovery procedure. In our work, we include anisotropy effects to the recently introduced constitutive relation derivation path, which has already been proved to be effective for non-prismatic and functionally graded material beams [6, 4, 5, 8].

Numerical examples will demonstrate that the proposed beam model describes the behavior of anisotropic structural elements with a good accuracy and far less computational effort. In particular, the proposed beam model effectively and accurately predicts: (i) the highly non-linear distribution of axial stresses, obtained despite a linear strain distribution and linear-elastic material behavior is assumed, (ii) the explicit dependency of horizontal stress on transversal internal force and load, (iii) the anisotropy influence on beam displacements, which is higher than that produced by shear deformation.

The outline of the paper is as follows: Section 2 defines the problem and illustrates the beam model ODEs, Section 3 derives the ODEs analytical solution, Sections 4 and 5 discuss some meaningful examples, and Section 6 resumes main properties, advantages, and limitations of the proposed method and delineates future research.

2. Beam model

In this section, we first introduce the 2D linear elastic problem, then we discuss the beam compatibility and equilibrium equations. Finally, the recovery of cross-section stress distributions and the beam constitutive relations are described.

2.1. 2D linear elastic problem

The beam *longitudinal axis* L and the beam *cross-section* H are closed and bounded subsets of x- and y- axes defined as

$$L := \{x \in [0, l]\}; \quad H := \{y \in [-\beta h, (1-\beta)\, h]\} \tag{1}$$

where l, h, and $0 < \beta < 1$ are the *beam length*, the *beam thickness*, and a reduction factor of h to define the distance between the x-axis and the lower boundary of the cross-section, respectively. The *beam depth* b denotes the cross-section size in the z-coordinate and, in the following, we assume $b = 1$. As illustrated in Figure 1, the 2D *beam body* Ω is defined as

$$\Omega := L \times H \tag{2}$$

Finally, we assume that the body is slender (i.e., $l \gg h$) and behaves under the plane stress and small displacements hypotheses.

We introduce the *displacement* vector field $\boldsymbol{u}(x, y) = [u_x(x, y), u_y(x, y)]$, the *stress* tensor field $\boldsymbol{\sigma}(x, y) = [\sigma_x(x, y), \sigma_y(x, y), \tau(x, y)]^T$, and the *strain* tensor field $\boldsymbol{\varepsilon}(x, y) = [\epsilon_x(x, y), \epsilon_y(x, y), \gamma_{xy}(x, y)]^T$ using the

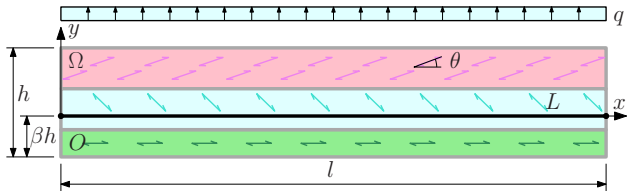

Figure 1: Anisotropic multi-layer beam with arbitrary orientation of principal directions: Geometry, coordinate system, dimensions and adopted notations of the considered problem.

Voigt notation. Furthermore, a *distributed load* $\boldsymbol{f} = [f_x, f_y]$ is applied on the domain Ω and suitable Boundary Conditions (BCs) are assigned on the boundary of Ω. The 2D compatibility PDEs read

$$\epsilon_x(x,y) = u_{x,x}(x,y) \tag{3a}$$
$$\epsilon_y(x,y) = u_{y,y}(x,y) \tag{3b}$$
$$\gamma_{xy}(x,y) = \frac{1}{2}\left(u_{x,y}(x,y) + u_{y,x}(x,y)\right) \tag{3c}$$

where the notation $(\cdot)_{,i}$ for $i = x, y$ represents a partial derivative. The 2D equilibrium PDEs read

$$\sigma_{x,x}(x,y) + \tau_{,y}(x,y) = -f_x(x,y) \tag{4a}$$
$$\tau_{,x}(x,y) + \sigma_{y,y}(x,y) = -f_y(x,y) \tag{4b}$$

The beam is made of a linear-elastic anisotropic material. As represented in Figure 1, the material properties of each layer do not vary with the beam axis and are piece-wise constant over the beam thickness. According to the notation introduced by Murakami et al. [36], the following 2D anisotropic constitutive relations hold:

$$\epsilon_x(x,y) = \frac{\sigma_x(x,y)}{E_{xx}(y)} + \frac{\sigma_y(x,y)}{E_{xy}(y)} + \frac{\tau(x,y)}{G_x(y)} \tag{5a}$$
$$\epsilon_y(x,y) = \frac{\sigma_x(x,y)}{E_{xy}(y)} + \frac{\sigma_y(x,y)}{E_{yy}(y)} + \frac{\tau(x,y)}{G_y(y)} \tag{5b}$$
$$\gamma_{xy}(x,y) = \frac{\sigma_x(x,y)}{G_x(y)} + \frac{\sigma_y(x,y)}{G_y(y)} + \frac{\tau(x,y)}{G(y)} \tag{5c}$$

The coefficients of the material constitutive relations can be collected in a matrix $\boldsymbol{D}$ that is defined as

$$\boldsymbol{D}(y) = \begin{bmatrix} \frac{1}{E_{xx}(y)} & \frac{1}{E_{xy}(y)} & \frac{1}{G_x(y)} \\ \frac{1}{E_{xy}(y)} & \frac{1}{E_{yy}(y)} & \frac{1}{G_y(y)} \\ \frac{1}{G_x(y)} & \frac{1}{G_y(y)} & \frac{1}{G(y)} \end{bmatrix} = \boldsymbol{R}^T(y) \begin{bmatrix} \frac{1}{E_{11}(y)} & -\frac{\nu(y)}{E_{11}(y)} & 0 \\ -\frac{\nu(y)}{E_{11}(y)} & \frac{1}{E_{22}(y)} & 0 \\ 0 & 0 & \frac{1}{G_{12}(y)} \end{bmatrix} \boldsymbol{R}(y) \tag{6}$$

where $\boldsymbol{R}(y)$ is defined as

$$\boldsymbol{R}(y) = \begin{bmatrix} \cos^2(\theta(y)) & \sin^2(\theta(y)) & 2\sin(\theta(y))\cos(\theta(y)) \\ \sin^2(\theta(y)) & \cos^2(\theta(y)) & -2\sin(\theta(y))\cos(\theta(y)) \\ -\sin(\theta(y))\cos(\theta(y)) & \sin(\theta(y))\cos(\theta(y)) & \cos^2(\theta(y)) - \sin^2(\theta(y)) \end{bmatrix} \tag{7}$$

$E_{11}(y), E_{22}(y), G_{12}(y)$, and $\nu(y)$ are the parameters defining the mechanical properties of the material with respect to the principal directions. The quantity $\theta(y)$, with $-\pi/2 < \theta(y) < \pi/2$, is the rotation of the principal direction of the material with respect to the x-axis.

Remark 2.1. *Due to the definition (6), $E_{xx}(y)$, $E_{xy}(y)$, $E_{yy}(y)$, and $G(y)$ are even functions of the material principal direction rotation $\theta(y)$ whereas the material coupling terms $G_x(y)$ and $G_y(y)$ are odd functions of θ.*

2.2. Compatibility and equilibrium ODEs

For convenience, we define the *axial stiffness* A^*, the dimensionless parameter β introduced in Equation (1), and the *bending stiffness* I^*

$$A^* = \int_H E_{xx}(y)\, dy; \quad \beta = \frac{1}{hA^*}\int_H E_{xx}(y)\, y\, dy; \quad I^* = \int_H E_{xx}(y)\, y^2\, dy \tag{8}$$

Remark 2.2. *Due to Definition (8), the origin of the adopted cartesian coordinate system O coincides with the so-called stiffness centroid that is equal to the cross-sectional geometric centroid only if the cross-section is symmetric and, in particular, when the beam is homogeneous, as discussed also by Kosmatka et al. [29].*

As usual for standard Timoshenko beam models, the 2D displacement field $\boldsymbol{u}(x,y) = [u_x(x,y), u_y(x,y)]^T$ is represented in terms of three 1D functions, indicated as *axial displacement* $u(x)$, *cross-section rotation* $\phi(x)$, and *transversal displacement* $v(x)$. Therefore, the displacement field components are approximated as follows

$$u_x(x,y) \approx u(x) - y\phi(x) \tag{9a}$$
$$u_y(x,y) \approx v(x) \tag{9b}$$

Introducing the *generalized strains* defined as the *axial strain* $\epsilon(x)$, the *curvature* $\chi(x)$, and the *shear strain* $\gamma(x)$, the beam compatibility is expressed through the following ODEs

$$\epsilon(x) = u'(x) \tag{10a}$$
$$\chi(x) = \phi'(x) \tag{10b}$$
$$\gamma(x) = v'(x) - \phi(x) \tag{10c}$$

where the notation $(\cdot)'$ denotes derivatives with respect to x.

Remark 2.3. *In light of Remark 2.2, kinematic approximation (9) differs from standard Timoshenko one. In fact, $u(x)$ represents the axial displacement of the stiffness centroid and, in general, it does not coincide with the mean value of the cross-section axial displacements (i.e., $u(x) = u_x(x,0) \neq 1/h \int_H u_x(x,y)\, dy$). Similarly, $\epsilon(x)$ is not the mean value of the axial strain evaluated within the cross-section, but just represents the axial elongation evaluated at $y = 0$ (i.e., $\epsilon(x) \neq 1/h \int_H \partial u_x(x,y)/\partial x\, dy$).*

We introduce the *axial internal force* $N(x)$, the *bending moment* $M(x)$, and the *transversal internal force* $V(x)$ as follows

$$N(x) = \int_H \sigma_x(x,y)\, dy; \quad M(x) = \int_H \sigma_x(x,y)\,(-y)\, dy; \quad V(x) = \int_H \tau(x,y)\, dy \tag{11}$$

Furthermore, we assume that $f_x = 0$ and we introduce the transversal load q

$$q = \int_H f_y\, dy = hf_y \tag{12}$$

Considering axial, rotational, and transversal equilibrium of a infinitesimally-long beam segment, the equilibrium ODEs read

$$N'(x) = 0 \tag{13a}$$
$$M'(x) = -V(x) \tag{13b}$$
$$V'(x) = -q \tag{13c}$$

2.3. Recovery of cross-section stress distributions

The stress recovery is based on a recursive procedure summarized in Figure 2 that leads to define a distribution of stresses that satisfies the first constitutive relation (5a) and the first equilibrium PDE (4a). It is worth noting that we assume vanishing transversal stress, i.e., $\sigma_y(x,y) = 0$, aiming at the maximal simplicity of the model.

In order to implement the recursive procedure, it is convenient to isolate Equations (5a) and (4a) for the variables $\sigma_x(x,y)$ and $\tau(x,y)$, respectively

$$\sigma_x(x,y) = E_{xx}(y)\,\epsilon_x(x,y) - \frac{E_{xx}(y)}{G_x(y)}\tau(x,y) \tag{14}$$

$$\tau(x,y) = -\int_{-\beta h}^{y} \sigma_{x,x}(x,\hat{y})\,d\hat{y} \tag{15}$$

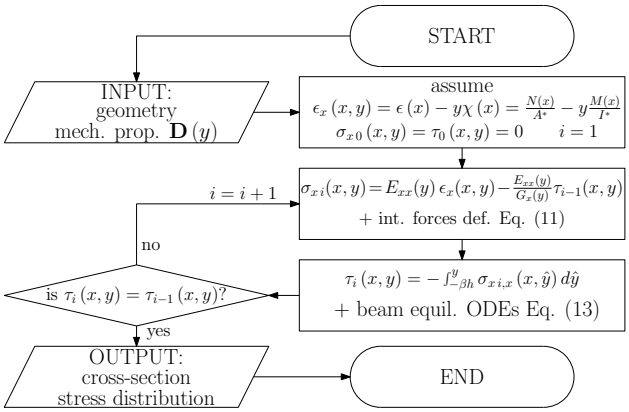

Figure 2: Flow chart of the iterative procedure adopted for the stress recovery.

The proposed iterative procedure leads to the following stress distributions:

$$\sigma_x(x,y) = d^N_{\sigma_x}(y)\,N(x) + d^M_{\sigma_x}(y)\,M(x) + d^V_{\sigma_x}(y)\,V(x) + d^q_{\sigma_x}(y)\,q \tag{16a}$$

$$\tau(x,y) = d^V_{\tau}(y)\,V(x) + d^q_{\tau}(y)\,q \tag{16b}$$

where

$$d^N_{\sigma_x}(y) = \frac{E_{xx}(y)}{A^*} \tag{17a}$$

$$d^M_{\sigma_x}(y) = -\frac{E_{xx}(y)}{I^*}y \tag{17b}$$

$$d^V_{\sigma_x}(y) = -\frac{E_{xx}(y)}{G_x(y)}d^V_{\tau}(y) + \int_H \frac{E_{xx}(y)}{G_x(y)}d^V_{\tau}(y)\,dy\,d^N_{\sigma_x}(y) - \int_H \frac{E_{xx}(y)}{G_x(y)}d^V_{\tau}(y)\,y\,dy\,d^M_{\sigma_x}(y) \tag{17c}$$

$$d^q_{\sigma_x}(y) = -\frac{E_{xx}(y)}{G_x(y)}d^q_{\tau}(y) + \int_H \frac{E_{xx}(y)}{G_x(y)}d^q_{\tau}(y)\,dy\,d^N_{\sigma_x}(y) - \int_H \frac{E_{xx}(y)}{G_x(y)}d^q_{\tau}(y)\,y\,dy\,d^M_{\sigma_x}(y) \tag{17d}$$

$$d^V_{\tau}(y) = \int_{-\beta h}^{y} d^M_{\sigma_x}(\hat{y})\,d\hat{y} \tag{17e}$$

$$d^q_{\tau}(y) = \int_{-\beta h}^{y} d^V_{\sigma_x}(\hat{y})\,d\hat{y} \tag{17f}$$

Remark 2.4. *In Definitions* (17c) *and* (17d)*, the second and the third addends allow Equation* (11) *to be satisfied, maintaining the standard physical meaning of beam model variables.*

Equation (16) highlights that both axial stress σ_x and shear stress τ_x explicitly depend on transversal internal force $V(x)$ and distributed load q. To the authors' knowledge, only Karttunen and Von Hertzen [28] and Hashin [23] obtained similar dependencies, but their analysis was limited to homogeneous beams. Furthermore, $d^V_{\sigma_x}$ and $d^q_{\sigma_x}$ depend on E_{xx}/G_x and E^2_{xx}/G^2_x, respectively (see Equation (17c) and (17d)); similar coefficients were reported also by Karttunen and Von Hertzen [28].

On the one hand, similarity of Equation (16) with analytical solutions reported in [28] and [23] suggests that the procedure summarized in Figure 2 may be effective. On the other hand, non-trivial dependency of σ_x on transversal internal force $V(x)$ indicates that stress recovery procedures developed for isotropic or orthotropic structural elements available in literature [16, 39, 44] and implemented in most of structural analysis commercial software can lead to coarse results when applied to anisotropic structural elements.

2.4. Beam constitutive relations

To complete the Timoshenko-like beam model, simplified constitutive relations have to be defined. To this aim, we introduce the stress potential

$$\Psi^*(x,y) = \frac{1}{2}\boldsymbol{\sigma}^T(x,y)\cdot\boldsymbol{D}(y)\cdot\boldsymbol{\sigma}(x,y) = \frac{1}{2}\left(\frac{\sigma_x^2(x,y)}{E_{xx}(y)} + \frac{\tau^2(x,y)}{G(y)} + 2\frac{\sigma_x(x,y)\,\tau(x,y)}{G_x(y)}\right) \tag{18}$$

Substituting the stress recovery relations (16) into Equation (18), the generalized strains result as the cross-section integral of the derivatives of the stress potential with respect to the corresponding internal forces, reading

$$\epsilon(x) = \int_H \frac{\partial\Psi^*(x,y)}{\partial N(x)}\,dy = \epsilon_N N(x) + \epsilon_M M(x) + \epsilon_V V(x) + \epsilon^q q \tag{19a}$$

$$\chi(x) = \int_H \frac{\partial\Psi^*(x,y)}{\partial M(x)}\,dy = \chi_N N(x) + \chi_M M(x) + \chi_V V(x) + \chi^q q \tag{19b}$$

$$\gamma(x) = \int_H \frac{\partial\Psi^*(x,y)}{\partial V(x)}\,dy = \gamma_N N(x) + \gamma_M M(x) + \gamma_V V(x) + \gamma^q q \tag{19c}$$

with

$$\epsilon_N = \int_H \frac{\left(d^N_{\sigma_x}(y)\right)^2}{E_{xx}(y)}\,dy \tag{20a}$$

$$\epsilon_M = \chi_N = \int_H \frac{d^N_{\sigma_x}(y)\,d^M_{\sigma_x}(y)}{E_{xx}(y)}\,dy = 0 \tag{20b}$$

$$\epsilon_V = \gamma_N = \int_H \frac{d^N_{\sigma_x}(y)\,d^V_{\sigma_x}(y)}{E_{xx}(y)}\,dy + \int_H \frac{d^N_{\sigma_x}(y)\,d^V_{\tau}(y)}{G_x(y)}\,dy \tag{20c}$$

$$\chi_M = \int_H \frac{\left(d^M_{\sigma_x}(y)\right)^2}{E_{xx}(y)}\,dy \tag{20d}$$

$$\chi_V = \gamma_M = \int_H \frac{d^M_{\sigma_x}(y)\,d^V_{\sigma_x}(y)}{E_{xx}(y)}\,dy + \int_H \frac{d^M_{\sigma_x}(y)\,d^V_{\tau}(y)}{G_x(y)}\,dy \tag{20e}$$

$$\gamma_V = \int_H \frac{\left(d^V_{\sigma_x}(y)\right)^2}{E_{xx}(y)}\,dy + \int_H \frac{d^V_{\sigma_x}d^V_{\tau}(y)}{G_x(y)}\,dy + \int_H \frac{\left(d^V_{\tau}(y)\right)^2}{G(y)}\,dy \tag{20f}$$

$$\epsilon^q = \int_H \frac{d^N_{\sigma_x}(y)\,d^q_{\sigma_x}(y)}{E_{xx}(y)}\,dy + \int_H \frac{d^N_{\sigma_x}(y)\,d^q_{\tau}(y)}{G_x(y)}\,dy \tag{20g}$$

$$\chi^q = \int_H \frac{d^M_{\sigma_x}(y)\,d^q_{\sigma_x}(y)}{E_{xx}(y)}\,dy + \int_H \frac{d^M_{\sigma_x}(y)\,d^q_{\tau}(y)}{G_x(y)}\,dy \tag{20h}$$

$$\gamma^q = \int_H \frac{d^V_{\sigma_x}(y)\,d^q_{\sigma_x}(y)}{E_{xx}(y)}\,dy + \int_H \frac{d^V_{\sigma_x}(y)\,d^q_{\tau}(y)}{G_x(y)}\,dy + \int_H \frac{d^q_{\sigma_x}(y)\,d^V_{\tau}(y)}{G_x(y)}\,dy + \int_H \frac{d^V_{\tau}(y)\,d^V_{\tau}(y)}{G(y)}\,dy \tag{20i}$$

Introducing the definitions of stress distributions (16a) into Definition (20b), we obtain that $\epsilon_M = \chi_N = 0$ due to the choice of the origin of the Cartesian coordinate system introduced in Equation (8). Conversely, the transversal internal force $V(x)$ produces not only shear strain $\gamma(x)$, but also axial strain $\epsilon(x)$ and curvature $\chi(x)$ since $\epsilon_V \neq 0$ and $\chi_V \neq 0$. Equations (20a) and (20d) lead to a definition of axial and bending stiffness analogous to the one obtained for isotropic beams. Conversely, Equation (20f) highlights that the shear stiffness of anisotropic beams γ_V depends not only on the shear modulus $G(y)$, but also on both the axial modulus of elasticity $E_{xx}(y)$ and the coupling term $G_x(y)$. Finally, all the generalized strains explicitly depend on the transversal load q (see Equation (19)).

Such a strong influence of the material anisotropy on beam constitutive relations is ignored by most of the literature. To the authors' knowledge, the coefficients $\epsilon_V = \gamma_N$ were analyzed only in [36, 37, 26, 41, 45], while the existence of the coefficients $\chi_V = \gamma_M$ was mentioned by [29] in the framework of the derivation of an enhanced 3D beam model, but their influence on the beam structural response was never analyzed.

Remark 2.5. *The extremely simple assumptions on kinematics (9) do not allow to tackle any higher order and boundary effects, as usual for all FSDT. Therefore, the proposed beam model has not the capability to describe deformation of the cross-section and the phenomena that occur in the neighborhood of constraints and concentrated loads.*

3. ODEs analytical solution

This section discusses the analytical solution of beam model ODEs (4), (10), and (19) for the bi-layer cantilever depicted in Figure 3. The two layers are made of the same anisotropic material and their thicknesses are $h_1 = \alpha h$ and $h_2 = (1-\alpha)h$ with $0 \leq \alpha \leq 1$. In the bottom layer, the material principal direction is aligned with the beam axis, therefore $E_{xx} = E_{11}$, $G = G_{12}$, and $1/G_x = 0$. In the top layer, the material principal direction is rotated with respect to the beam axis of an angle θ, therefore $E_{xx} = E_{11}/\mu$ and $G = G_{12}/\kappa$. The dimensionless parameters μ and κ account for the reduction of axial and shear modulus

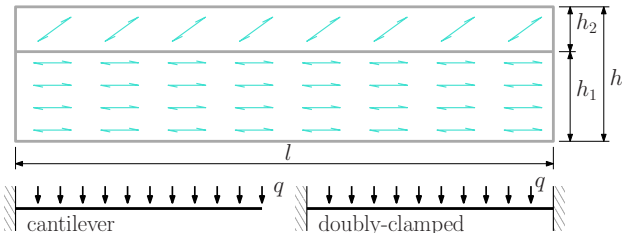

Figure 3: Bi-layer anisotropic cantilever. Geometry, loads, and BCs.

due to the rotation θ of the material principal direction (6). They are defined in Appendix A, together with the material coupling term G_x. For $\alpha = 1$, the beam reduces to an homogeneous orthotropic beam with material orientation aligned with the beam axis. Conversely, for $\alpha = 0$, the beam reduces to a homogeneous anisotropic beam, similar to the one analyzed by [36, 37, 26, 41, 45, 23, 28]. Finally, aiming at the maximum simplicity of the analytical solution, we are going to neglect the influence of transversal load on the generalized strains (i.e., we assume $\epsilon^q = \chi^q = \gamma^q = 0$).

The coefficients of beam constitutive relations introduced in Definition (19) read

$$\epsilon_N = \frac{P_1}{E_{11}h}; \quad \epsilon_V = \gamma_N = -\frac{P_3}{G_x h}; \quad \chi_M = \frac{12P_2}{E_{11}h^3}; \quad \chi_V = \gamma_M = -\frac{18P_4}{G_x h^2}; \quad \gamma_V = \frac{6P_5}{5G_{12}h} + \frac{P_6 E_{11}}{5G_x^2 h} \tag{21}$$

where the dimensionless coefficients P_i for $i = 1 \dots 6$ (reported in Appendix B) account for the influence of geometry and material on the structural element stiffness.

The solution of ODEs (10), (4), and (19) leads to the following analytical expressions for beam model variables

$$\begin{aligned}
N(x) =& C_6 \\
V(x) =& -qx + C_5 \\
M(x) =& \frac{qx^2}{2} - C_5 x + C_3 \\
\phi(x) =& \overbrace{\frac{12P_2}{E_{11}h^3}\left(\frac{qx^3}{6} - \frac{C_5 x^2}{2} + C_3 x\right)}^{\phi_{EB}(x)} + \overbrace{\frac{18P_4}{G_x h^2}\left(-\frac{qx^2}{2} + C_5 x\right)}^{\phi_c(x)} + C_2 \\
v(x) =& \overbrace{\frac{12P_2}{E_{11}h^3}\left(\frac{qx^4}{24} - \frac{C_5 x^3}{6} + \frac{C_3 x^2}{2}\right)}^{v_{EB}(x)} + \overbrace{\frac{6P_5}{5G_{12}h}\left(-\frac{qx^2}{2} + C_5 x\right)}^{v_T(x)} \\
&+ \overbrace{\frac{P_3}{G_x h}C_6 x - \frac{18P_4}{G_x h^2}C_3 x}^{v_c(x)} + \overbrace{\frac{P_6 E_{11}}{G_x^2 h}\left(-\frac{qx^2}{2} + C_5 x\right)}^{v_r(x)} + C_2 x + C_1 \\
u(x) =& \overbrace{\frac{P_1}{E_{11}h}C_6 x}^{u_{EB}(x)} - \overbrace{\frac{P_3}{G_x h}\left(-\frac{qx^2}{2} + C_5 x\right)}^{u_c(x)} + C_4
\end{aligned} \tag{22}$$

where the C_i for $i = 1 \dots 6$ depend on BCs. Notations $(\cdot)_{EB}$, $(\cdot)_T$, $(\cdot)_c$, and $(\cdot)_r$ denote addends depending on the axial stiffness E_{11}, the shear stiffness G_{12}, the coupling term G_x, and the ratio G_x^2/E_{11}, respectively. Furthermore, few calculations lead to conclude that the addends denoted as $(\cdot)_{EB}$ coincide with the solution of the Euler Bernoulli (EB) beam theory, whereas the addend denoted as $(\cdot)_T$ coincides with the shear deformation considered by Timoshenko beam theory.

Considering a cantilever beam (see Figure 3), the following BCs are enforced

$$u(0) = 0; \quad \phi(0) = 0; \quad v(0) = 0; \quad N(l) = 0; \quad M(l) = 0; \quad V(l) = 0 \tag{23}$$

Requiring ODEs solution (22) to satisfy BCs (23) leads to the following values

$$C_1 = C_2 = C_4 = C_6 = 0; \quad C_3 = \frac{ql^2}{2}; \quad C_5 = ql \tag{24}$$

Finally, introducing the dimensionless parameter $\lambda = l/h$, the maximum transversal displacement of the beam reads

$$v(l) = v_{EB}(l) + v_T(l) + v_c(l) + v_r(l) = \frac{3ql\lambda^3}{2E_{11}}Q_1 + \frac{3ql\lambda}{G_{12}}Q_2 - \frac{9ql\lambda^2}{G_x}Q_3 + \frac{ql\lambda}{G_x}\frac{E_{11}}{G_x}Q_4 \tag{25}$$

where the dimensionless coefficients Q_i for $i = 1 \dots 4$ are reported in Appendix C.

Equation (25) shows that the maximum transversal displacement $v(l)$ is obtained by the sum of four terms. The first addend $v_{EB}(l)$ depends on the Young's modulus along the principal direction E_{11} and, for $\alpha = 1$, it corresponds to the classical EB solution. The second addend $v_T(l)$ depends on the shear modulus G_{12} and, for $\alpha = 1$, it coincides with the contribution due to shear deformation handled by the Timoshenko beam model. The third term $v_c(l)$ depends on the material coupling term G_x and its existence is just a consequence of the fact that the material principal directions are not aligned with the beam axis. The fourth term $v_r(l)$ depends on the material coupling term G_x and on the ratio E_{11}/G_x that appears in the definition of axial stress (see Equation (17c)).

Looking at Equation (25) from a different perspective, the first addend, $v_{EB}(l)$, depends on λ^3, $v_T(l)$ and $v_r(l)$ depend on λ, while $v_c(l)$ depends on λ^2. The highlighted result are in agreement with statements in standard literature: shear deformation $v_T(l)$ has a negligible influence on the total displacement of slender beams (i.e., for $\lambda \gg 1$). However, the term $v_c(l)$ can weigh on the total displacement more than the shear deformation whereas the forth term $v_r(l)$ can have an influence similar to the shear deformation. To the authors' knowledge, the existence of terms $v_c(l)$ and $v_r(l)$ was never mentioned in the literature and their role will be analyzed in the following section.

Finally, it is worth mentioning that

- stress distributions (16) reduce to linear and quadratic functions for $\alpha = 1$ and $1/G_x = 0$, as usual in homogeneous prismatic beams,
- $\epsilon_N = 1/(E_{11}h)$, $\epsilon_V = \gamma_N = \chi_V = \gamma_M = 0$, $\chi_M = 12/\left(h^3 E_{11}\right)$, and $\gamma_V = 6/(5G_{12}h)$ for $\alpha = 1$, analogously to homogeneous prismatic isotropic beams,
- $\epsilon_N = \mu/(E_{11}h)$, $\epsilon_V = \gamma_N = 1/(G_x h)$, $\chi_M = 12\mu/\left(h^3 E_{11}\right)$, $\chi_V = \gamma_M = 0$, and $\gamma_V = 6\kappa/(5G_{12}h)$ for $\alpha = 0$, similarly to the anisotropic beam model proposed by Murakami et al. [36],

confirming that the presented beam model can recover analytical solutions already available in literature.

However, the proposed beam model can handle an arbitrary number of layers, which implies a quickly growing complexity of the analytical solution making numerical tools the only possible way to solve problems involving complex geometries. The present paper discusses only a bi-layer geometry, being sufficient to show the main peculiarities of anisotropic beams and the model capabilities.

4. Comparison with analytical solution, homogeneous beam

This section compares the solution of the beam model discussed in Section 2 with the analytical solution derived in [28] for a simply supported homogeneous beam. The results are obtained assuming the following parameters

$$\begin{gathered} h = 0.2\,\text{mm}; \quad l = 2\,\text{mm}; \quad q = 1\,\text{N/mm}; \quad \alpha = 0 \\ E_{11} = 10^4\,\text{MPa}; \quad E_{22} = 5 \cdot 10^2\,\text{MPa}; \quad G = 10^3\,\text{MPa}; \quad \nu = 0.25 \end{gathered} \tag{26}$$

It is worth mentioning that the material is highly anisotropic: $E_{11}/E_{22} = 20$ and $E_{11}/G = 10$. Such a choice aims at magnifying the effects of both shear deformation and coupling on the behavior of the structural element, allowing for a more accurate discussion of the proposed beam model effectiveness.

Assuming $\theta = 45$ deg, the rotation of the constitutive relation (6) implies

$$E_{xx} = E_{yy} = 1.904\,\text{GPa}; \qquad E_{xy} = 40.000\,\text{GPa}; \qquad G_x = G_y = -1.052\,\text{GPa}; \qquad G = 0.322\,\text{GPa} \tag{27}$$

Figure 4 compares cross-section distributions of stresses: in the following, superscript *mod* is used for the analytical solution computed by means of ODEs (10), (4), and (19), superscript ref stands for the reference solution computed using the analytical expression reported in [28], while the superscript T is used for the stress recovery procedure developed for the isotropic Timoshenko beam.

The results demonstrate that the proposed beam model provides results substantially identical to the reference solution. In particular, Figure 4(b) highlights that shear does not vanish in the beam mid-span $\tau(l/2, y) \neq 0$, despite the vertical internal force vanishes $V(l/2) = 0$. Further comments about this peculiarity of simply supported beams can be found in [28]. More interestingly, Figure 4(e) highlights that axial stress does not vanish at the bearing $\sigma_x(l, y) \neq 0$, despite both bending moment and axial internal force vanish $M(l) = N(l) = 0$. Considering also Figures 4(c) and 4(d), it is possible to conclude that anisotropy influences the distribution of both axial and shear stresses. In particular, stress-recovery procedures developed for isotropic structural elements can underestimate the maximum axial stress by more than 10 %.

5. Comparison with 2D FE, bi-layer beam

This section reports results for two examples: the cantilever beam already introduced in Section 3 and the doubly-clamped beam shown in Figure 3. In both cases, results are obtained assuming the following parameters

$$\begin{gathered} h = 100\,\text{mm}; \quad q = 1\,\text{N/mm}; \quad \alpha = 0.5 \\ E_{11} = 10^4\,\text{MPa}; \quad E_{22} = 5 \cdot 10^2\,\text{MPa}; \quad G = 10^3\,\text{MPa}; \quad \nu = 0 \end{gathered} \tag{28}$$

In this section, the reference solution is computed using the commercial software Abaqus [13], and, in particular, discretizing the 2D problem domain Ω with a structured mesh of 4 node plane stress, fully integrated, bilinear elements CPS4. As discussed in Section 1, the structural element behavior can be affected by boundary effects, which cannot be handled by the proposed beam model (Remark 2.5).

Aiming at limiting their influence on the reference solution, the BCs are imposed requiring only vanishing mean value of cross-section displacements and rotation. In this manner, constrained cross-sections can warp and deform, but stress concentrations are limited in magnitude. A mesh convergence analysis has been performed choosing progressively decreasing element size δ according to the series $1/2^n$ for $n = 0, 1, 2, \ldots$. We finally adopted mesh elements characterized by $\delta = 0.25$mm, leading to a relative maximum displacement magnitude smaller than 10^{-4}.

Transversal displacement $v^{ref}(x)$ and shear strain $\gamma^{ref}(x)$ have been obtained by computing the mean value over the cross-section of the 2D transversal displacements $u_y^{ref}(x, y)$ and shear strains $\gamma_{xy}^{ref}(x, y)$, respectively. Conversely, axial $N^{ref}(x)$ and shear $V^{ref}(x)$ internal forces have been obtained as the integral over the cross-section of stress components $\sigma_x^{ref}(x, y)$ and $\tau^{ref}(x, y)$, respectively. The bending moment $M^{ref}(x)$ has been obtained as the integral over the cross section of axial stress $\sigma_x^{ref}(x, y)$ times the y coordinate. Finally, according to Remark 2.3, the axial displacement $u^{ref}(x)$ and the rotation $\phi^{ref}(x)$ have been computed as the coefficients of the linear least squares with respect to y of the axial displacements $u_x^{ref}(x, y)$. Similarly, the axial strain $\epsilon^{ref}(x)$ and the curvature $\chi^{ref}(x)$ have been computed as the coefficients of the linear least squares with respect to y of the strains $\epsilon_x^{ref}(x, y)$.

5.1. Cantilever beam

In the following we set $l = 500\,\text{mm}$, i.e., we choose $\lambda = 5$. This assumption leads to a beam geometry that is close to the well known limit of validity of the FSDTs and, therefore, it will allow potential issues of the proposed model to be identified. Assuming $\theta = 15$ deg, the rotation of constitutive relation (6) leads to

$$\mu = 1.5853; \quad \kappa = 1.2750; \quad G_x = -4.2222 \cdot 10^3\,\text{MPa} \tag{29}$$

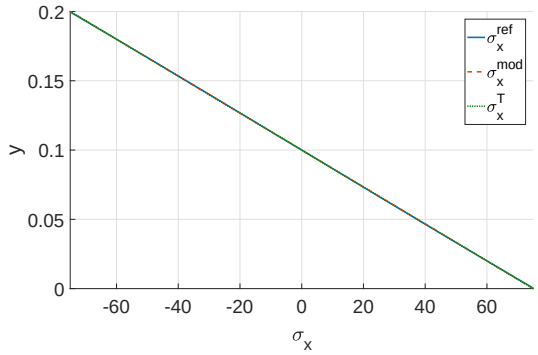

(a) axial stress, $x = 1$

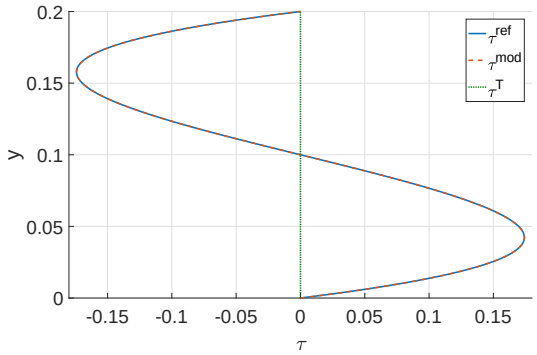

(b) shear stress, $x = 1$

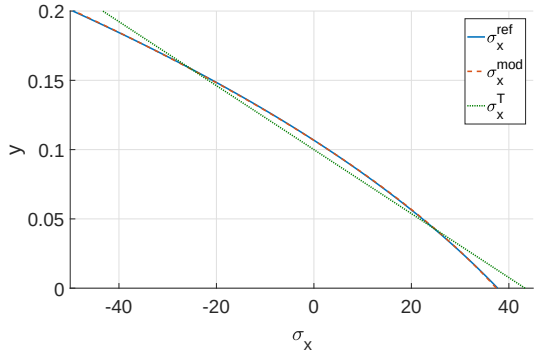

(c) axial stress, $x = 1.65$

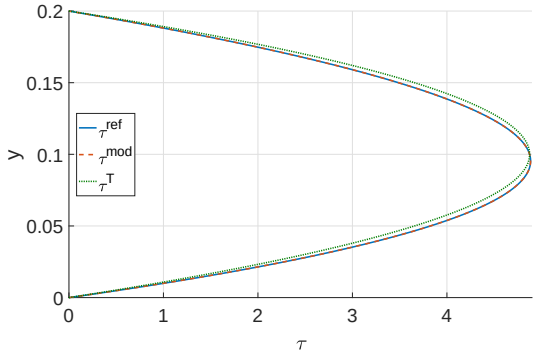

(d) shear stress, $x = 1.65$

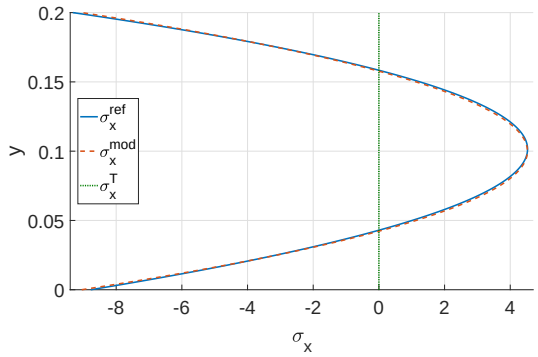

(e) axial stress, $x = 2$

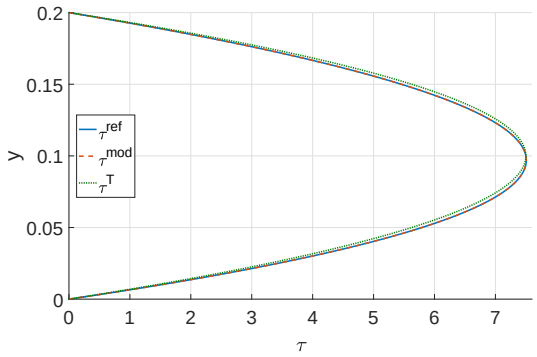

(f) shear stress, $x = 2$

Figure 4: Homogeneous, simply-supported, anisotropic beam ($\theta = 45$ deg). Analysis of cross-section stress distributions: Comparisons among reference (*ref*), proposed beam model (*mod*), and Timoshenko (*T*) solutions.

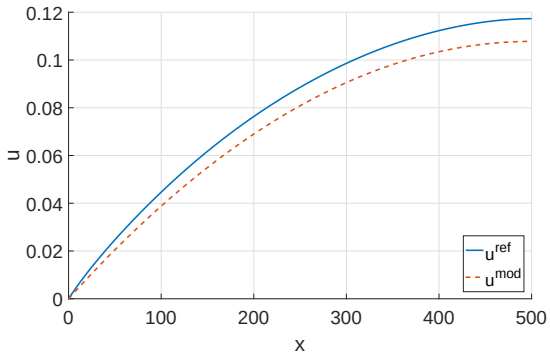

(a) axial displacement

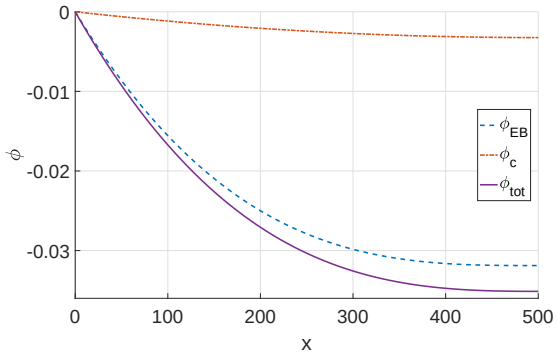

(b) rotation components

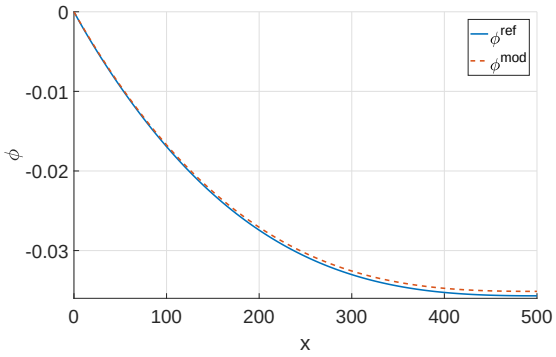

(c) rotation

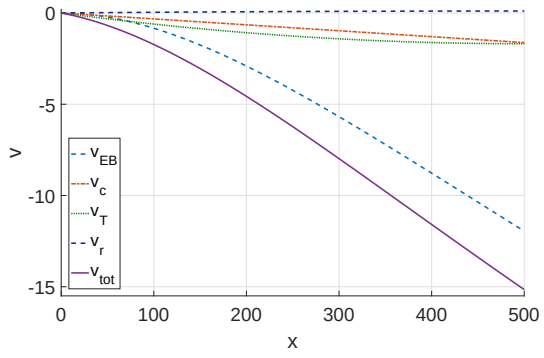

(d) transversal displacement components

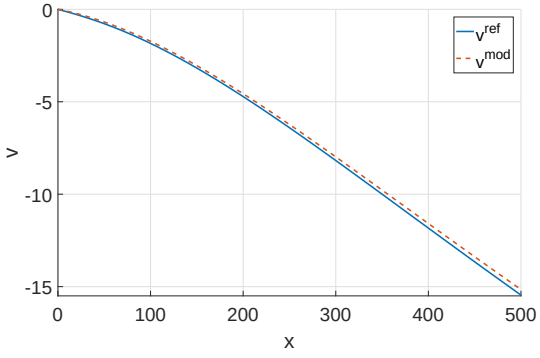

(e) transversal displacement

Figure 5: Bi-layer anisotropic cantilever ($\theta = 15$ deg). Analysis of the generalized displacements components according to the proposed beam model (Figures 5(b) and 5(d)). Comparison between the proposed beam model and the reference solution (Figures 5(a), 5(c), and 5(e)).

Figure 5 reports displacement results. Figures 5(b) and 5(d) analyze the model solution, highlighting the significant influence of the material coupling term G_x on the global structural response. In particular, Figure 5(d) shows that the transversal displacement component $v_c(x)$ (see Equation (22)) has a magnitude similar to the shear deformation component $v_T(x)$ and it contributes to total transversal displacement more than 10 %, while $v_r(x)$ influences the total displacement less than 1 %. Figure 5(b) highlights that $\phi_c(x)$ contributes to total cross-section rotation up to 10 %. Figures 5(c) and 5(e) reveal a good accuracy of the proposed model. Indeed, relative errors are smaller than 2 % for rotation and transversal displacements.

Due to considered loads $N^{mod}(x) = 0$ and, due to BCs, also $u_{EB}(x) = 0$ (see Equation (22)). As a consequence, $u^{mod}(x) = u_c(x)$ i.e., the axial displacement is uniquely controlled by the material coupling term G_x and the transversal internal force $V(x)$. Figure 5(a) shows that the beam model correctly predicts a non-vanishing distribution of axial displacement, with an error of about 8 %. Nevertheless, the axial displacement is two order of magnitude smaller than the transversal one, not affecting the errors evaluated on the total displacement $\boldsymbol{u}(x, y)$.

Figure 6 reports results concerning generalized strains. Figure 6(a) shows that axial strain is uniquely attributed to the transversal internal force $V(x)$ by means of the coefficient ϵ_V as already discussed above (see also Figure 5(a)). The comparison with the reference solution (Figure 6(b)) confirms the good prediction quality provided by the beam model. Anyway, the reference solution reveals the presence of some boundary effects close to the clamp that can not be detected by the proposed beam model (see Remark 2.5) and may also be responsible for the discrepancies on axial displacements.

Figure 6(c) shows that the transversal internal force $V(x)$ produces a non-negligible curvature, accounting for up to 10 % of the total curvature. Similarly, Figure 6(e) shows that the bending moment $M(x)$ strongly influences the shear strain. Indeed, shear strain has a non-linear distribution despite transversal internal force $V(x)$ is linear. In particular, the bending moment $M(x)$ accounts for up to 30 % of the total shear strain. For both shear strain and curvature, Figures 6(d) and 6(f) demonstrate that the beam model and the reference solutions are in very good agreement. Only near to the clamp, the reference solution reveals the presence of some boundary effects that can not be described by the beam model.

Figures 7 and 8 report cross-section stress distributions at $1/2l = 250\,\text{mm}$ and $3/4l = 375\,\text{mm}$.

Figures 7(a) and 7(c) highlight that the axial stress depending on the transversal internal force $d^V_{\sigma_x}(y)\,V(x)$ is not negligible at all, but can increase the magnitude of maximum stress up to 30 %. Conversely, the effect of the axial stress depending on the transversal load $d^q_{\sigma_x}(y)\,q$ is less significant. The comparison with the reference solution (Figures 7(b) and 7(d)) reveals that the stress recovery developed in Section 2.3 provides accurate estimations of the stress magnitude, with relative errors usually below 10 %. In particular, the stress recovery correctly predicts the jump of axial stress at the inter-layer surface. Conversely, the reference solution reveals the presence of some boundary effects near to the free end of the cantilever beam that the proposed model is not able to capture (see Remark 2.5), and may locally lead to an increase of the relative errors up to 40 %.

Figures 8(a) and 8(c) highlight that the shear stress depending on transversal load $d^q_\tau(y)\,q$ is not negligible, but it can lead to the creation of a local minimum on the inter-layer surface. The comparison with the reference solution (Figures 8(a) and 8(c)) reveals that the proposed stress recovery leads to good results, with relative errors usually below 5 %.

In order to complete the discussion of the proposed model capabilities, Tables 1, 2, and 3 compare the solutions obtained using different models. Maximum displacements $\psi(l)$, with $\psi = u, \phi, v$, are evaluated using 2D FE ($\psi^{ref}(l)$), standard EB beam model ($\psi^{EB}(l)$), and the proposed beam model ($\psi^{mod}(l)$). Only for the transversal displacement, also the Timoshenko beam model is considered since its solution differs from EB ($v^{EB}(l) + v^T(l)$). Relative errors are computed as

$$e^i = \frac{\left|\psi^i(l) - \psi^{ref}(l)\right|}{\left|\psi^{ref}(l)\right|} \text{ with } i = EB, T, mod \tag{30}$$

Finally, results and relative errors are provided for $\lambda = 5$, 10, and 20 and $\theta = \pm 15$ deg.

If, on one side, the relative errors obtained by all models decrease with increasing slenderness of the considered beams, consistently with standard beam model assumptions, on the other side, it is worth

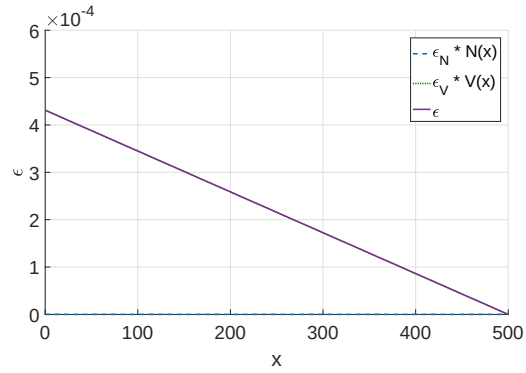

(a) axial strain components

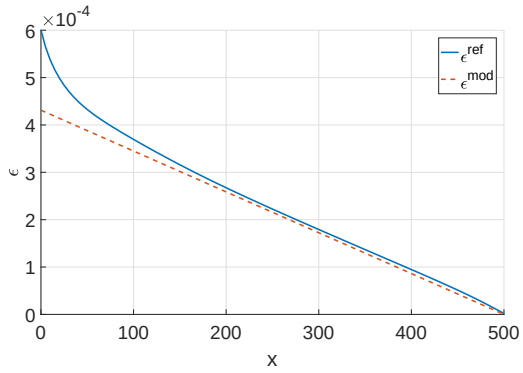

(b) axial strain

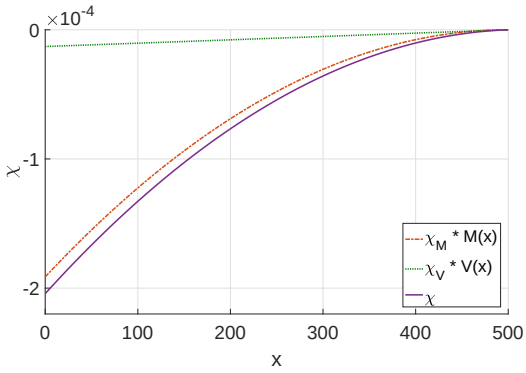

(c) curvature components

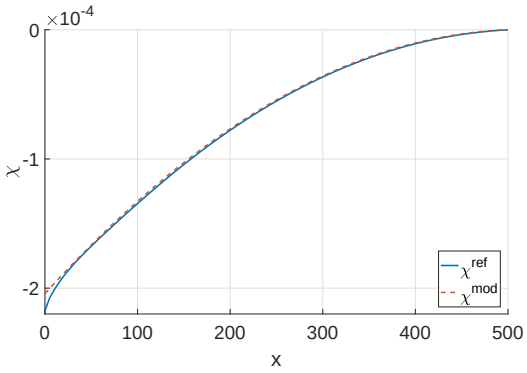

(d) curvature

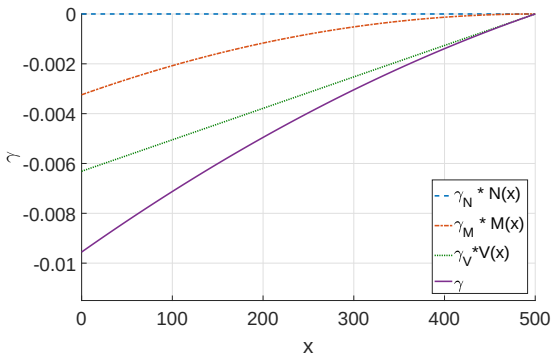

(e) shear strain components

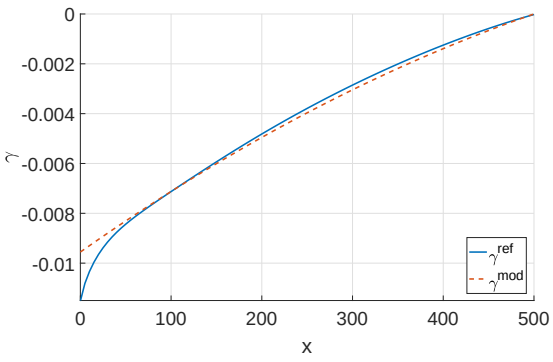

(f) shear strain

Figure 6: Bi-layer anisotropic cantilever ($\theta = 15$ deg). Analysis of the generalized strains components according to the proposed beam model (Figures 6(a), 6(c), and 6(e)). Comparison between the proposed beam model and the reference solution (Figures 6(b), 6(d), and 6(f)).

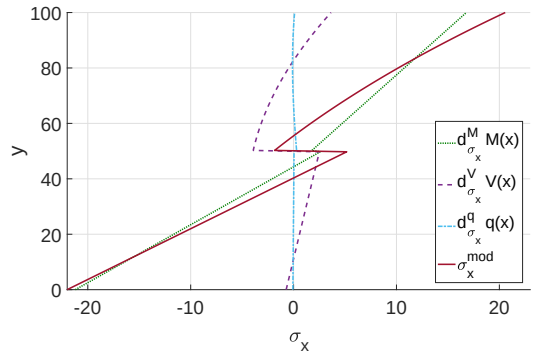

(a) axial stress components, $x = 250$

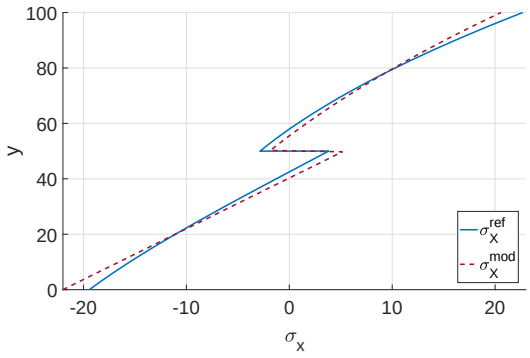

(b) axial stress, $x = 250$

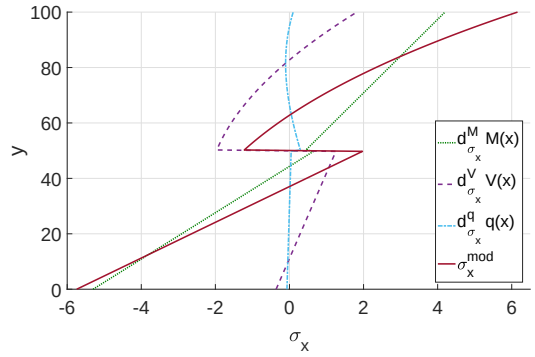

(c) axial stress components, $x = 375$

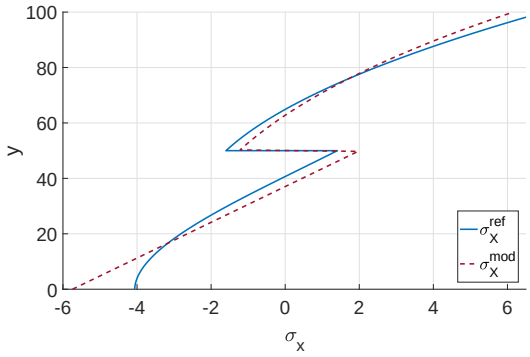

(d) axial stress, $x = 375$

Figure 7: Bi-layer anisotropic cantilever ($\theta = 15$ deg). Axial stress distributions evaluated at $x = 250$ mm (Figures 7(a) and 7(b)), and $x = 375$ mm (Figures 7(c) and 7(d)). Analysis of the axial stress components according to the proposed beam model (Figures 7(a) and 7(c)) and comparison between the proposed beam model and the reference solution (Figures 7(b) and7(d)).

λ	θ [deg]	u^{ref} [mm]	u^{EB} [mm]	u^{mod} [mm]	e_u^{EB} [%]	e_u^{mod} [%]
5	+15	1.173e–1	0.000e+0	1.078e–1	100	8.10
5	–15	–1.125e–1	0.000e+0	–1.078e–1	100	4.18
10	+15	4.612e–1	0.000e+0	4.311e–1	100	6.53
10	–15	–4.504e–1	0.000e+0	–4.311e–1	100	4.29
20	+15	1.828e+0	0.000e+0	1.724e+0	100	5.69
20	–15	–1.803e+0	0.000e+0	–1.724e+0	100	4.38

Table 1: Bi-layer anisotropic cantilever. Maximum axial displacement $u\,(l)$ evaluated according to EB u^{EB} and proposed u^{mod} beam models and relative errors.

λ	θ [deg]	ϕ^{ref} [rad]	ϕ^{EB} [rad]	ϕ^{mod} [rad]	e_ϕ^{EB} [%]	e_ϕ^{mod} [%]
5	+15	–3.569e–2	–3.189e–2	–3.513e–2	10.6	1.57
5	–15	–2.841e–2	–3.189e–2	–2.864e–2	12.2	0.81
10	+15	–2.706e–1	–2.551e–1	–2.681e–1	5.73	0.92
10	–15	–2.410e–1	–2.551e–1	–2.421e–1	5.85	0.46
20	+15	–2.103e+0	–2.041e+0	–2.093e+0	2.95	0.48
20	–15	–1.984e+0	–2.041e+0	–1.989e+0	2.87	0.25

Table 2: Bi-layer anisotropic cantilever. Maximum rotations $\phi\,(l)$ evaluated according to EB ϕ^{EB} and proposed ϕ^{mod} beam models and relative errors.

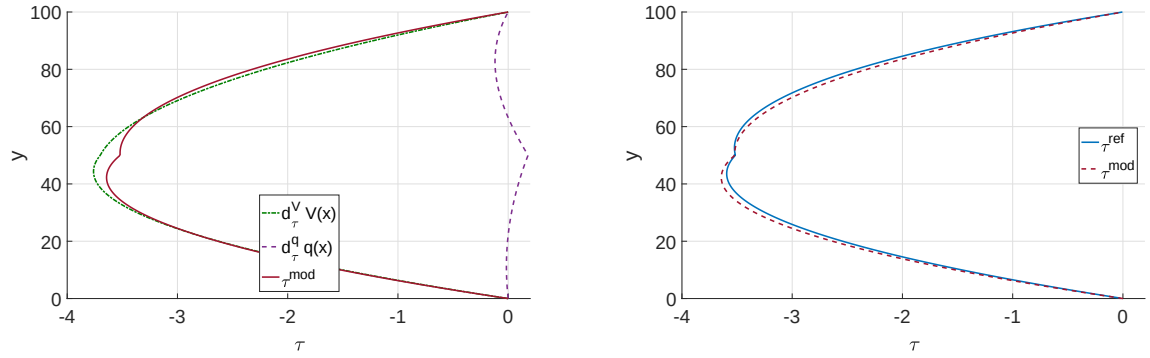

(a) shear stress components, $x = 250$

(b) shear stress, $x = 250$

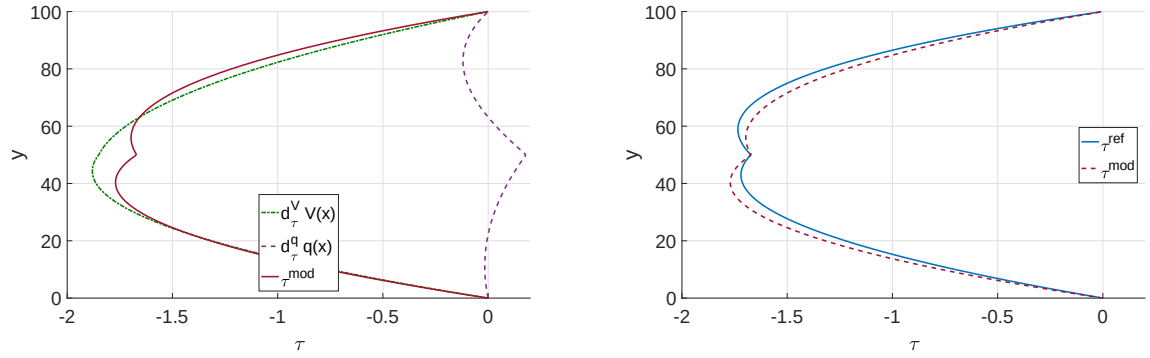

(c) shear stress components, $x = 375$

(d) shear stress, $x = 375$

Figure 8: Bi-layer anisotropic cantilever ($\theta = 15$ deg). Shear stress distributions evaluated at $x = 250$ mm (Figures 8(a) and 8(b)), and $x = 375$ mm (Figures 8(c) and 8(d)). Analysis of the shear stress components according to the proposed beam model (Figures 8(a) and 8(c)) and comparison between the proposed beam model and the reference solution (Figures 8(b) and8(d)).

λ	θ [deg]	v^{ref} [mm]	v^{EB} [mm]	$v^{EB} + v^{T}$ [mm]	v^{mod} [mm]	e_v^{EB} [%]	e_v^{EB+T} [%]	e_v^{mod} [%]
5	+15	−1.545e+1	−1.196e+1	−1.364e+1	−1.516e+1	22.6	11.7	1.88
5	−15	−1.177e+1	−1.196e+1	−1.364e+1	−1.191e+1	1.61	15.9	1.19
10	+15	−2.130e+2	−1.913e+2	−1.981e+2	−2.106e+2	10.2	7.00	1.13
10	−15	−1.834e+2	−1.913e+2	−1.981e+2	−1.847e+2	4.31	8.02	0.71
20	+15	−3.210e+3	−3.061e+3	−3.088e+3	−3.190e+3	4.64	3.80	0.62
20	−15	−2.972e+3	−3.061e+3	−3.088e+3	−2.982e+3	2.99	3.90	0.34

Table 3: Bi-layer anisotropic cantilever. Maximum transversal displacements v (l) evaluated according to EB v^{EB}, Timoshenko v^{T}, and proposed v^{mod} beam models and relative errors.

highlighting that EB and Timoshenko beam models lead to errors that are often greater than 10 % and are therefore not acceptable even in the area of applied engineering design. On the contrary, the proposed beam model leads to errors that are usually smaller than 2 %, reaching an accuracy adequate for applied engineering design concepts. Table 1 highlights that our model estimates the axial displacement $u(x)$ with errors near 5 %. Anyway, the magnitude of axial displacements is two orders of magnitude smaller than other cross-section displacement, therefore, the relative error on axial displacement might not have a strong influence on the magnitude of the displacement $\boldsymbol{u}(x, y)$.

Furthermore, Table 3 highlights that the Timoshenko beam model not always performs better than EB, even when considering thick beams. In particular, for $\lambda = 5$ and $\theta = -15$ deg, the maximum transversal displacement predicted by the proposed beam model qualitatively coincides with the EB solution i.e., $v^{mod}(l) \approx v^{EB}(l)$. On the one hand, such a result highlights (i) the strong influence of fiber direction on the structural element stiffness (see Remark 2.1) and (ii) the inappropriateness of beam models developed for isotropic structural elements. On the other hand, the extremely low errors obtained for both positive and negative θ confirm the effectiveness of the proposed model in handling all peculiar aspects of anisotropic beams.

Finally, Figure 9 reports the weight of the four components $v_{EB}(l)$, $v_T(l)$, $v_c(l)$, and $v_r(l)$ on the total transversal displacement as a function of λ. The analysis is limited to geometric features and mechanical

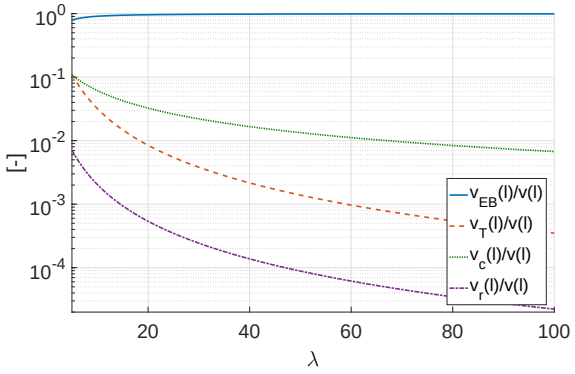

Figure 9: Bi-layer anisotropic cantilever ($\theta = 15$ deg). Incidence of the maximum transversal displacement components $v_{EB}(l)$, $v_T(l)$, $v_c(l)$, and $v_r(l)$ evaluated for varying λ.

material properties introduced at the beginning of Section 5, but it highlights several effects of the anisotropy on the structural response of beams. The component $v_c(l)$, depending on the material coupling term G_x, is always bigger than the component depending on the shear $v_T(l)$. As an example, considering $\lambda = 20$ $v_c(l)/v(l) > 3\,\%$ whereas $v_T(l)/v(l) < 1\%$. Furthermore, for $\lambda = 80$ $v_c(l)/v(l) \approx 1\,\%$ whereas $v_T(l)/v(l) \approx 0.05\,\%$. As a consequence, we can conclude that the material coupling contribution $v_c(x)$ is significant also for slender structural elements, while shear contribution is negligible. The transversal displacement $v_r(l)$ always contributes to the total displacement less than 1 %.

5.2. Doubly-clamped beam

This section considers the statically indeterminate bi-layer beam depicted in Figure 3, aiming at confirming the capabilities of the proposed beam model in effectively estimating the anisotropic beam stiffness. The analytical solution reported in Equation (22) is still valid. Conversely, the following BCs have to be considered:

$$u(0) = u(l) = 0; \quad \phi(0) = \phi(l) = 0; \quad v(0) = v(l) = 0 \tag{31}$$

The analytical expression for the coefficients C_i, for $i = 1 \dots 6$, turns out to be extremely complex and, for brevity, they will not be reported. Anyway, all the coefficients depend on all mechanical properties E_{11}, G_{12}, and G_x. As a consequence, the subdivision of displacements in components $(\cdot)_{EB}$, $(\cdot)_T$, $(\cdot)_c$, and

$(\cdot)_r$ introduced in Equation (22) is no longer meaningful and will not be considered in the following. We set $l = 1000\,\text{mm}$ and we use the geometrical and mechanical properties reported in Equations (28) and (29).

Figure 10 reports results concerning distributions of internal forces $N(x)$, $M(x)$, and $V(x)$. Such results

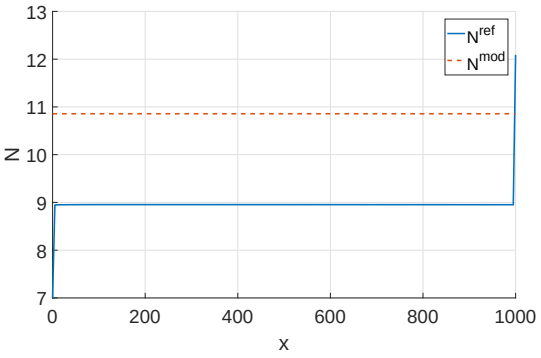

(a) axial internal force

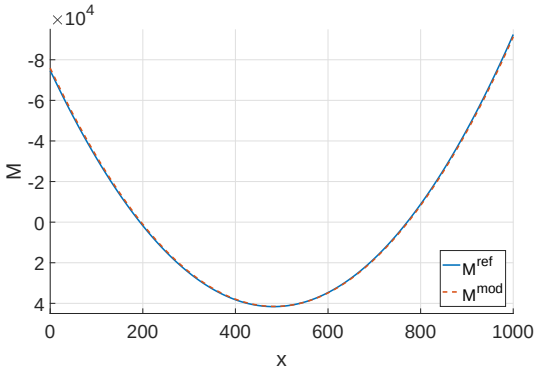

(b) bending moment

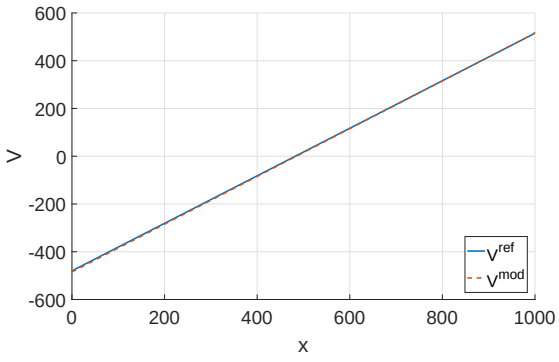

(c) transversal internal force

Figure 10: Doubly clamped bi-layer anisotropic beam. Analysis of internal forces. Comparison between the proposed beam model and the reference solutions.

highlight a non-trivial effect of the material anisotropy. The distribution of internal forces is non-symmetric and reactions corresponding to the clamp on the right are higher than those on the left clamp, despite BCs and load are symmetric with respect to the beam mid-span. Once more, comparison with the reference solution reveals the high accuracy of the proposed beam model that predicts both bending moment and transversal internal force with negligible errors. Finally, the proposed beam model correctly predicts a non-vanishing, constant distribution of axial internal force, which magnitude is anyway negligible when compared to the transversal internal force and bending moment.

Tables 4, 5, and 6 report constraint reactions (i.e., $N(x)$, $M(x)$, and $V(x)$ for $x = 0, l$) evaluated using 2D FE, standard EB beam model, and the proposed beam model for $\lambda = 5,\ 10,$ and 20. Relative errors are computed according to Equation (30).

As already remarked in Section 5.1, EB beam model leads to errors that are often bigger than 10 %, leading to estimates that are too coarse for efficient engineering designs. Conversely, the proposed beam model leads to errors that are generally three to six times smaller and usually below 2 %. Only Table 4 highlights that our model estimates axial internal force $N(x)$ with errors over 20 %. Anyway, since the magnitude of axial internal force is approximately 50 times smaller than the transversal one, the relative error on axial internal force might not have a strong influence on the global response of the structural element.

λ	x	N^{ref} [N]	N^{EB} [N]	N^{mod} [N]	e_N^{EB} [%]	e_N^{mod} [%]
5	0	7.356e+0	0.000e+0	8.742e+0	100	18.8
5	l	7.356e+0	0.000e+0	8.742e+0	100	18.8
10	0	8.959e+0	0.000e+0	1.092e+1	100	21.9
10	l	8.959e+0	0.000e+0	1.092e+1	100	21.9
20	0	9.472e+0	0.000e+0	1.165e+1	100	23.0
20	l	9.472e+0	0.000e+0	1.165e+1	100	23.0

Table 4: Doubly clamped bi-layer anisotropic beam. Axial constraint reactions $N(0)$ and $N(l)$ evaluated according to EB N^{EB} and proposed N^{mod} beam models and relative errors.

λ	x	M^{ref} [Nm]	M^{EB} [Nm]	M^{mod} [Nm]	e_M^{EB} [%]	e_M^{mod} [%]
5	0	–1.732e+4	–2.083e+4	–1.794e+4	20.3	3.58
5	l	–2.482e+4	–2.083e+4	–2.415e+4	16.1	2.70
10	0	–7.458e+4	–8.333e+4	–7.583e+4	11.7	1.68
10	l	–9.244e+4	–8.333e+4	–9.137e+4	9.86	1.16
20	0	–3.138e+5	–3.333e+5	–3.170e+5	6.21	1.02
20	l	–3.526e+5	–3.333e+5	–3.502e+5	5.47	0.68

Table 5: Doubly clamped bi-layer anisotropic beam. Bending moment constraint reactions $M(0)$ and $M(l)$ evaluated according to EB M^{EB} and proposed M^{mod} beam models and relative errors.

λ	x	V^{ref} [N]	V^{EB} [N]	V^{mod} [N]	e_V^{EB} [%]	e_V^{mod} [%]
5	0	–2.333e+2	–2.500e+2	–2.376e+2	7.16	1.84
5	l	–2.645e+2	–2.500e+2	–2.624e+2	5.48	0.79
10	0	–4.817e+2	–5.000e+2	–4.845e+2	3.80	0.58
10	l	–5.184e+2	–5.000e+2	–5.155e+2	3.55	0.56
20	0	–9.921e+2	–1.000e+3	–9.834e+2	0.80	0.88
20	l	–1.026e+2	–1.000e+3	–1.017e+3	2.53	0.88

Table 6: Doubly clamped bi-layer anisotropic beam. Shear constraint reactions $V(0)$ and $V(l)$ evaluated according to EB V^{EB} and proposed V^{mod} beam models and relative errors.

6. Conclusions

In this paper we have proposed a simple beam model able to effectively handle the influence of anisotropy on the beam constitutive relations and on the corresponding stress distributions. The independent variables of the model are the internal forces and the standard Timoshenko kinematic parameters. Despite its simplicity, the beam model has allowed to highlight the following peculiarities of anisotropic beams.

1. Material anisotropy leads the transversal internal force to contribute up to 30 % to the magnitude of axial stress, strongly affecting also beam strength, not explicitly considered in this paper.
2. In beam constitutive relations, non-vanishing out-of-diagonal terms that relate the transversal internal force with the curvature (and the bending moment with the shear strain) exist and influence the response of the structural element more than 10 %.
3. In addition to the standard bending contribution (proportional to cube beam-slenderness) and the shear one (proportional to beam-slenderness), a third term, depending on the material coupling term and proportional to the square beam-slenderness, contributes up to 10 % to the transversal displacement.
4. The contribution depending on material coupling terms can be more significant than the contribution from shear deformation and it may not be negligible for length-vs-thickness ratios greater than 50.

A systematic comparison with analytical results and 2D FE solutions, obtained using highly refined meshes, demonstrates the effectiveness of the proposed modeling approach. In general, the proposed beam model has a computational cost similar to the simplest beam models used in engineering practice and it is able to predict significant displacements and internal forces with relative errors usually smaller than 2 %. On the contrary, coarse adaptations of beam models developed for isotropic structural elements may lead to errors greater than 20 % in the prediction of both internal forces and displacements. Furthermore, analysis of stress distributions demonstrates that stress recovery tools developed for isotropic structural elements are no longer effective for anisotropic ones, but ad-hoc routines need to be developed. The main limitations of the proposed model are the assumptions on kinematics that do not allow to describe higher order and boundary effects.

Future research will include (i) the development and analysis of suitable numerical discretization for the beam model proposed in this paper, (ii) the application of the proposed modeling strategy to 3D beams and plates, and (iii) the generalization of the model in order to include higher order and size effects.

7. Acknowledgments

This work was funded by the Austrian Science Found (FWF) [M 2009-N32]. F. Auricchio and S. Morganti would like to acknowledge the strategic theme of the University of Pavia "Virtual Modeling and Additive Manufacturing for Advanced Materials (3D@UniPV)"

Appendix A. Mechanical properties coefficients

$$\mu = E_{11}\cos^2(\theta)\left(\frac{(2\nu+1)\cos^2(\theta)-2\nu}{E_{11}}+\frac{1}{E_{22}}\left(\cos^2(\theta)-2+\frac{1}{\cos^2(\theta)}\right)\right)+\frac{1-\cos^2(\theta)}{G_{12}} \tag{A.1}$$

$$\kappa = 4G_{12}\cos^2(\theta)\left(\frac{(2\nu+1)\left(1-\cos^2(\theta)\right)}{E_{11}}+\frac{1-\left(\cos^2(\theta)\right)}{E_{22}}+\frac{1}{G_{12}}\left(\cos^2(\theta)-1+\frac{1}{4\cos^2(\theta)}\right)\right) \tag{A.2}$$

$$\frac{1}{G_x} = 2\sin(\theta)\cos(\theta)\left(\frac{\left((2\nu+1)\cos^2(\theta)-\nu\right)}{E_{11}}+2\frac{\left(\cos^2(\theta)-1\right)}{E_{22}}+\frac{\left(1-2\cos^2(\theta)\right)}{G_{12}}\right) \tag{A.3}$$

Appendix B. Dimensionless coefficients P_i (for $i = 1 \dots 6$)

$$P_1 = \frac{\mu}{1 + (\mu - 1)\,\alpha} \tag{B.1}$$

$$P_2 = \frac{\mu\,(1 + (\mu - 1)\,\alpha)}{1 + (\mu - 1)\,\alpha\,((\mu - 1)\,\alpha^3 + 4\alpha^2 - 6\alpha + 4)} \tag{B.2}$$

$$P_3 = \frac{\left(-1 + (\mu - 1)\,\alpha^2 + (-4\mu + 2)\,\alpha\right)(\alpha - 1)^2}{(1 + (\mu - 1)\,\alpha)\,(1 + (\mu - 1)\,\alpha\,((\mu - 1)\,\alpha^3 + 4\alpha^2 - 6\alpha + 4))} \tag{B.3}$$

$$P_4 = \frac{\mu^2\alpha^2\,(\alpha - 1)^2}{(1 + (\mu - 1)\,\alpha\,((\mu - 1)\,\alpha^3 + 4\alpha^2 - 6\alpha + 4))^2} \tag{B.4}$$

$$\begin{aligned} P_5 =& \frac{1}{(1 + (\mu - 1)\,\alpha\,((\mu - 1)\,\alpha^3 + 4\alpha^2 - 6\alpha + 4))^2} \\ & \Big((\mu - 1)^2\left(\mu^2 - \kappa\right)\alpha^7 - \left(3\mu^2 - 10\mu\kappa + 7\kappa\right)(\mu - 1)\,\alpha^6 \\ & + \left(5\mu^3 + (1 - 40\kappa)\,\mu^2 + 55\mu\kappa - 21\kappa\right)\alpha^5 + \left((70\kappa - 15)\,\mu^2 - 90\mu\kappa + 35\kappa\right)\alpha^4 \\ & + \left((10 - 55\kappa)\,\mu^2 + 80\mu\kappa - 35\kappa\right)\alpha^3 + \kappa\,(16\mu - 21)\,(\mu - 1)\,\alpha^2 + 7\kappa\,(\mu - 1)\,\alpha + \kappa\Big) \end{aligned} \tag{B.5}$$

$$\begin{aligned} P_6 =& \frac{(\alpha - 1)^3}{((\mu - 1)\,\alpha\,((\mu - 1)\,\alpha^3 + 4\alpha^2 - 6\alpha + 4) + 1)^3\,\mu}\Big(1 + (6\mu - 1)\,(\mu - 1)^3\,\alpha^8 \\ & + \left(-42\mu^4 + 129\mu^3 - 140\mu^2 + 61\mu - 8\right)\alpha^7 + \left(96\mu^4 - 372\mu^3 + 429\mu^2 - 181\mu + 28\right)\alpha^6 \\ & + \left(622\mu^3 - 736\mu^2 + 305\mu - 56\right)\alpha^5 + \left(-609\mu^3 + 719\mu^2 - 315\mu + 70\right)\alpha^4 \\ & + \left(249\mu^3 - 372\mu^2 + 199\mu - 56\right)\alpha^3 + \left(79\mu^2 - 71\mu + 28\right)\alpha^2 + (11\mu - 8)\,\alpha\Big) \end{aligned} \tag{B.6}$$

Appendix C. Maximum displacement coefficients Q_i (for $i = 1 \dots 3$)

$$\begin{aligned} Q_1 =& \frac{\mu}{(1 + (\mu - 1)\,\alpha\,((\mu - 1)\,\alpha^3 + 4\alpha^2 - 6\alpha + 4))^2}\Big((\mu - 1)^3\,\alpha^5 + 5\,(\mu - 1)^2\,\alpha^4 \\ & + 2\left(-3\mu^2 + 8\mu - 5\right)\alpha^3 + 2\,(2\mu - 5)\,(\mu - 1)\,\alpha^2 + 5\,(\mu - 1)\,\alpha + 1\Big) \end{aligned} \tag{C.1}$$

$$\begin{aligned} Q_2 =& \frac{1}{5\,(1 + (\mu - 1)\,\alpha\,((\mu - 1)\,\alpha^3 + 4\alpha^2 - 6\alpha + 4))^2}\Big((\mu - 1)^2\left(\mu^2 - \kappa\right)\alpha^7 - \left(3\mu^2 - 20\mu\kappa + 7\kappa\right)(\mu - 1)\,\alpha^6 \\ & + \left(5\mu^3 - (40\kappa - 1)\,\mu^2 + 55\mu\kappa - 21\kappa\right)\alpha^5 + 5\left((14\kappa - 3)\,\mu^2 - 18\mu\kappa + 7\kappa\right)\alpha^4 - \\ & 5\left((11\kappa - 2)\,\mu^2 - 16\mu\kappa + 7\kappa\right)\alpha^3 + \kappa\,(\mu - 1)^2\,\alpha^2 + 7\kappa\,(\mu - 1)\,\alpha + \kappa\Big) \end{aligned} \tag{C.2}$$

$$Q_3 = \frac{-\mu^2\alpha^2\,(\alpha - 1)^2}{(1 + (\mu - 1)\,\alpha\,((\mu - 1)\,\alpha^3 + 4\alpha^2 - 6\alpha + 4))^2} \tag{C.3}$$

$$\begin{aligned} Q_4 =& \frac{(\alpha - 1)^3}{10\,((\mu - 1)\,\alpha\,((\mu - 1)\,\alpha^3 + 4\alpha^2 - 6\alpha + 4) + 1)^3\,\mu}\Big(1 + (6\mu - 1)\,(\mu - 1)^3\,\alpha^8 \\ & + \left(-42\mu^4 + 129\mu^3 - 140\mu^2 + 61\mu - 8\right)\alpha^7 + \left(96\mu^4 - 372\mu^3 + 429\mu^2 - 181\mu + 28\right)\alpha^6 \\ & + \left(622\mu^3 - 736\mu^2 + 305\mu - 56\right)\alpha^5 + \left(-609\mu^3 + 719\mu^2 - 315\mu + 70\right)\alpha^4 \\ & + \left(249\mu^3 - 372\mu^2 + 199\mu - 56\right)\alpha^3 + \left(79\mu^2 - 71\mu + 28\right)aa^2 + (11\mu - 8)\,\alpha\Big) \end{aligned} \tag{C.4}$$

References

[1] Aifantis, E. C. (1999). Gradient deformation models at nano, micro, and macro scales. *Journal of Engineering Materials and Technology 121*(2), 189–202.

[2] Askes, H. and E. C. Aifantis (2011). Gradient elasticity in statics and dynamics: an overview of formulations, length scale identification procedures, finite element implementations and new results. *International Journal of Solids and Structures 48*(13), 1962–1990.

[3] Auricchio, F., G. Balduzzi, and C. Lovadina (2010). A new modeling approach for planar beams: Finite-element solutions based on mixed variational derivations. *Journal of Mechanics of Materials and Structures 5*, 771–794.

[4] Balduzzi, G., M. Aminbaghai, F. Auricchio, and J. Füssl (2018). Planar Timoshenko-like model for multilayer non-prismatic beams. *International Journal of Mechanics and Materials in Design 14*(1), 51–70.

[5] Balduzzi, G., M. Aminbaghai, and J. Füssl (2017). Linear response of a planar FGM beam with non-linear variation of the mechanical properties. In A. Güemes, A. Benjeddou, J. Rodellar, and J. Leng (Eds.), *SMART 2017*, pp. 1285–1294. CIMNE.

[6] Balduzzi, G., M. Aminbaghai, E. Sacco, J. Füssl, J. Eberhardsteiner, and F. Auricchio (2016). Non-prismatic beams: a simple and effective Timoshenko-like model. *International Journal of Solids and Structures 90*, 236–250.

[7] Balduzzi, G., G. Kandler, and J. Füssl (2018). Estimation of GLT beam stiffness based on homogenized board mechanical properties and composite beam theory. In *Proceedings of the 6th European Conference on Computational Mechanics (ECCM 6)*, Glasgow, UK.

[8] Balduzzi, G., E. Sacco, F. Auricchio, and J. Füssl (2017). Non-prismatic thin-walled beams: critical issues and effective modeling. In L. Ascione, V. Berardi, L. Feo, F. Fraternali, and A. M. Tralli (Eds.), *AIMETA2017 XXIII conference of the Italian Association of Theoretical and Applied Mechanics*.

[9] Bauchau, O. A. (1985). A beam theory for anisotropic materials. *Journal of Applied Mechanics 52*(2), 416–422.

[10] Bruhns, O. T. (2003). *Advanced Mechanics of Solids*. Springer.

[11] Carrera, E. and A. Ciuffreda (2005). A unified formulation to assess theories of multilayered plates for various bending problems. *Composite structures 69*, 271–293.

[12] Choi, I. and C. Horgan (1977). Saint-venant's principle and end effects in anisotropic elasticity. *Journal of Applied Mechanics 44*(3), 424–430.

[13] Dassault Systemes, 2014 (2014). *Abaqus/CAE User's Guide - Release 6.16*. Providence, RI, USA.: Dassault Systemes, 2014.

[14] Dong, S., C. Alpdogan, and E. Taciroglu (2010). Much ado about shear correction factors in Timoshenko beam theory. *International Journal of Solids and Structures 47*, 1651–1665.

[15] Dong, S. B., J. B. Kosmatka, and H. C. Lin (2001). On Saint-Venant's problem for an inhomogeneous, anisotropic cylinder - part I: methodology for Saint-Venant solutions. *ASME, Journal of Applied Mechanics 68*, 376–381.

[16] Dufour, J.-E., P. Antolin, G. Sangalli, F. Auricchio, and A. Reali (2018). A cost-effective isogeometric approach for composite plates based on a stress recovery procedure. *Composites Part B: Engineering 138*, 12–18.

[17] Garcea, G., R. Gonçalves, A. Bilotta, D. Manta, R. Bebiano, L. Leonetti, D. Magisano, and D. Camotim (2016). Deformation modes of thin-walled members: A comparison between the method of generalized eigenvectors and generalized beam theory. *Thin-Walled Structures 100*, 192–212.

[18] Genoese, A., A. Genoese, A. Bilotta, and G. Garcea (2014a). Buckling analysis through a generalized beam model including section distortions. *Thin-Walled Structures 85*, 125–141.

[19] Genoese, A., A. Genoese, A. Bilotta, and G. Garcea (2014b). A generalized model for heterogeneous and anisotropic beams including section distortions. *Thin-Walled Structures 74*, 85–103.

[20] Groh, R. and P. Weaver (2014). Buckling analysis of variable angle tow, variable thickness panels with transverse shear effects. *Composite Structures 107*, 482–493.

[21] Groh, R. and P. M. Weaver (2016). A computationally efficient 2D model for inherently equilibrated 3D stress predictions in heterogeneous laminated plates. Part I: model formulation. *Composite structures 156*, 186–217.

[22] Gupta, M., D. Sarojini, A. Shah, and D. H. Hodges (2018). Dimensional reduction technique for analysis of aperiodic inhomogeneous structures. In *2018 AIAA/ASCE/AHS/ASC Structures, Structural Dynamics, and Materials Conference*.

[23] Hashin, Z. (1967). Plane anisotropic beams. *Journal of Applied Mechanics 34*(2), 257–262.

[24] Horgan, C. O. and L. A. Carlsson (2018). *Comprehensive composite materials II*, Volume 7, Chapter Saint-Venant end effects for anisotropic materials, pp. 38–55. Oxfor Academic Press.

[25] Jourawski, D. (1856). Sur le résistance d'un corps prismatique et d'une piece composée en bois ou on tôle de fer à une force perpendiculaire à leur longeur. In *Annales des Ponts et Chaussées*, Volume 12, pp. 328–351.

[26] Jung, S. N., V. Nagaraj, and I. Chopra (2002). Refined structural model for thin- and thick- walled composite rotor blades. *AIAA journal 40*(1), 105–116.

[27] Kandler, G., J. Füssl, E. Serrano, and J. Eberhardsteiner (2015). Effective stiffness prediction of glt beams based on stiffness distributions of individual lamellas. *Wood Science and Technology 49*(6), 1101–1121.

[28] Karttunen, A. T. and R. Von Hertzen (2016). On the foundations of anisotropic interior beam theories. *Composites Part B: Engineering 87*, 299–310.

[29] Kosmatka, J. B., H. C. Lin, and S. B. Dong (2001). On Saint-Venant's problem for an inhomogeneous, anisotropic cylinder - part II: cross-sectional properties. *ASME, Journal of Applied Mechanics 68*, 382–391.

[30] Ladeveze, P. and J. Simmonds (1998). New concepts for linear beam theory with arbitrary geometry and loading. *European Journal of Mechanics, A/solids 17*, 377–402.

[31] Lekhnitskiĭ, S. (1968). *Anisotropic plates*. Gordon and Breach.

[32] Lin, H. C., S. B. Dong, and J. B. Kosmatka (2001). On Saint-Venant's problem for an inhomogeneous, anisotropic cylinder - part III: end effects. *ASME, Journal of Applied Mechanics 68*, 392–398.
[33] Lukacevic, M., G. Kandler, M. Hu, A. Olsson, and J. Füssl (2019). A 3d model for knots and related fiber deviations in sawn timber for prediction of mechanical properties of boards. *Materials & Design 166*, 107617.
[34] Mascia, N. T. and L. Vanalli (2012). Evaluation of the coefficients of mutual influence of wood through off-axis compression tests. *Construction and Building Materials 30*, 522–528.
[35] Mascia, N. T., L. Vanalli, R. R. Paccola, and M. R. Scoaris (2010). Mechanical behaviour of wood beams with grain orientation. *Mecánica Computacional XXIX*, 2839–2854.
[36] Murakami, H., E. Reissner, and J. Yamakawa (1996). Anisotropic beam theories with shear deformation. *Journal of Applied Mechanics 63*(3), 660–668.
[37] Murakami, H. and J. Yamakawa (1996). On approximate solutions for the deformation of plane anisotropic beams. *Composites Part B: Engineering 27*(5), 493–504.
[38] Parandoush, P. and D. Lin (2017). A review on additive manufacturing of polymer-fiber composites. *Composite Structures 182*, 36–53.
[39] Patton, A., J.-E. Dufour, P. Antolin, and A. Reali (2019). Fast and accurate elastic analysis of laminated composite plates via isogeometric collocation and an equilibrium-based stress recovery approach. *Composite Structures*, 111026.
[40] Pech, S., G. Kandler, M. Lukacevic, and J. Füssl (2019). Metamodel assisted optimization of glued laminated timber systems by reordering wooden lamellas using metaheuristic algorithms. *Engineering Applications of Artificial Intelligence 79*, 129–141.
[41] Qin, Z. and L. Librescu (2002). On a shear-deformable theory of anisotropic thin-walled beams: further contribution and validations. *Composite Structures 56*(4), 345–358.
[42] Rajagopal, A. (2014). *Advancements in rotor blade cross-sectional analysis using the variational-asymptotic method*. Ph. D. thesis, Georgia Institute of Technology.
[43] Silvestre, N. and D. Camotim (2002). First-order generalised beam theory for arbitrary orthotropic materials. *Thin-Walled Structures 40*(9), 755–789.
[44] Tornabene, F., N. Fantuzzi, M. Bacciocchi, and J. Reddy (2017). A posteriori stress and strain recovery procedure for the static analysis of laminated shells resting on nonlinear elastic foundation. *Composites Part B: Engineering 126*, 162–191.
[45] Vanalli, L., N. T. Mascia, and R. R. Paccola (2003). Influence of the anisotropy on the mechanical behavior of laminated beams. In *Proceedings of COBEM 2003*.
[46] Vidal, P., L. Gallimard, and O. Polit (2012). Composite beam finite element based on the proper generalized decomposition. *Computers & Structures 102*, 76–86.
[47] Yu, W., D. H. Hodges, V. Volovoi, and C. E. Cesnik (2002). On Timoshenko-like modeling of initially curved and twisted composite beams. *International Journal of Solids and Structures 39*, 5101–5121.
[48] Yun, W., V. Volovoi, D. H. Hodges, and X. Hong (2002). Validation of the variational asymptotic beam sectional analysis (VABS). *AIAA (American Institute of Aeronautics and Astronautics) journal 40*, 2105–2113.